

Angle-resolved photoelectron study of the valence levels of BF_3 in the range $17 \leq h\nu \leq 28$ eV

J. L. Dehmer

Argonne National Laboratory, Argonne, Illinois 60439

A. C. Parr and S. H. Southworth

Synchrotron Ultraviolet Radiation Facility, National Bureau of Standards, Washington, D.C. 20234

D. M. P. Holland*

Institute of Physical Science and Technology, University of Maryland, College Park, Maryland 20742

(Received 30 April 1984)

Photoelectron branching ratios and angular distributions have been measured for the six outermost levels of BF_3 in the range $17 \leq h\nu \leq 28$ eV with the use of synchrotron radiation. Comparisons are made with a recent multiple-scattering model calculation which indicates that a shape resonance in the e' electronic continuum should appear in five of the six channels studied. Good agreement between experiment and theory is found in a majority of the comparisons; however, experimental evidence for the expected e' shape resonance is clear in some cases but absent in others. The results are discussed in the context of other cases in which shape resonances, well known from inner-shell spectra, are obscured in valence-shell properties. Experiments which would help clarify the role of the e' shape resonance in the photoionization dynamics of BF_3 are suggested.

I. INTRODUCTION

The role of shape resonances in molecular photoionization has been avidly studied over the last dozen years or so (see, e.g., Ref. 1). Indeed, shape resonances have now been identified in tens of molecules, and their manifestations in electronic and vibrational partial cross sections and photoelectron angular distributions have been satisfactorily understood and semiquantitatively reproduced in several cases. Nevertheless, our understanding of shape resonances in valence-shell spectra is still very tentative, even though we often know the symmetries and approximate spectral locations of shape resonances for a given molecule from inner-shell spectra.

An example will serve to illustrate the point. In SF_6 , the sulfur $L_{2,3}$ spectra²⁻⁷ show extremely intense t_{2g} and e_g shape resonances lying ~ 3 and ~ 15 eV above the L -shell ionization limit. Since these are quasibound states in the respective continua (i.e., a final-state effect), it is reasonable to expect that these same states would be prominent in valence-shell photoionization channels in which they are dipole-allowed. A shift of 1 to 4 eV to higher kinetic energy is to be expected due to differences in screening between core and valence-shell vacancies. In fact, the t_{2g} is observed⁸⁻¹⁰ in the $1t_{2u}$, $5t_{1u}$, and $4t_{1u}$ (dipole-allowed) photoionization channels, but it also appears with sizable strength in the $1t_{1g}$ and $3e_g$ channels, where it is dipole forbidden in the independent-electron approximation. This observation, attributed¹⁰ to continuum-continuum coupling, obscures the use of shape resonances to assign the symmetries of photoelectron peaks. Even more problematic, the e_g is not clearly seen in valence-shell partial cross sections^{8,9} at all. The cause for this is still unknown.

Several effects can complicate the role of shape reso-

nances in valence-shell processes relative to their more simple behavior in inner-shell spectra. Electron-correlation effects involving continuum-continuum coupling,¹⁰ interaction with autoionizing states,¹¹ and intrachannel coupling¹² are more likely owing to the closely spaced valence-shell ionization potentials (IP's) and the better overlap between valence-shell vacancies and shape resonances. The dipole matrix element for valence shells can exhibit stronger energy dependence, including zeros, than matrix elements involving compact core states. Vibronic coupling may be enhanced and, indeed, has been shown to cause a breakdown of the single-particle model for inner-valence processes.^{13,14} Hence, these and other unforeseen influences make the study of valence-shell photoionization dynamics richer and less well understood. These observations also underscore the importance of utilizing inner-shell data to establish the basic, unperturbed pattern of shape resonance features, before attempting to understand the valence-shell spectra.

In this paper, we present angle-resolved photoelectron data for the valence shells of BF_3 to investigate valence-shell photoionization dynamics in this highly-symmetric polyatomic molecule. This case was chosen because an e' shape resonance is firmly established^{4,15-21} to occur at ~ 2.2 eV kinetic energy in the boron K -shell spectrum and because comprehensive independent-electron calculations²⁰ have been carried out for all the subshells of BF_3 using the multiple-scattering model. Furthermore, as our analogous study¹⁰ on SF_6 clarified the role of the t_{2g} resonance in valence-shell photoionization in SF_6 , the comparative study of these two highly symmetric fluorides seemed promising. In fact, agreement between experiment and theory is very reasonable in many of the comparisons discussed below, indicating a realistic, first-order theoretical description.²⁰ However, a predicted shape-resonance

feature in the branching ratio for the $4e'$ channel is absent, possibly due to some of the reasons outlined above. These results are discussed in the context of the analogous study on SF_6 and future measurements are suggested to clarify the role of the e' resonance in valence-shell spectra of BF_3 .

II. EXPERIMENT

The apparatus used in this work has been described in detail elsewhere²² and will only be discussed briefly here. The variable wavelength light was obtained from a high-throughput, 2-m, normal-incidence monochromator²³ attached to the National Bureau of Standards (SURF-II) storage ring. With a 1200-line/mm grating, a virtual entrance slit (the stored electron beam, with a height of $\sim 80 \mu\text{m}$), and a 100- μm exit slit, this instrument produced a spectral resolution of 0.4 \AA full width at half maximum (FWHM) and a flux of 5×10^{10} photons $\text{sec}^{-1} \text{ \AA}^{-1}$ at 600 \AA with a typical 10-mA beam circulating in the storage ring. The ejected electrons were energy analyzed with a 2-in. mean-radius hemispherical analyzer operated with a constant resolution of $\sim 110 \text{ meV}$. The analyzer was calibrated for electron transmission as a function of kinetic energy and ejection angle by using Ar gas whose photoionization cross section²⁴ and photoelectron asymmetry parameters²⁵⁻²⁷ are known in this wavelength range. As the light from the monochromator was elliptically polarized, the differential cross section in the dipole approximation, assuming randomly oriented target molecules, can be written

$$\frac{d\sigma}{d\Omega} = (\sigma_{\text{tot}}/4\pi) [1 + \frac{1}{4}\beta(3P \cos 2\theta + 1)], \quad (1)$$

where β is the photoelectron asymmetry parameter, θ is the photoelectron ejection angle relative to the major polarization axis, and

$$P = (I_{||} - I_{\perp}) / (I_{||} + I_{\perp}) \quad (2)$$

is the polarization of the light which was measured with a three-mirror polarization analyzer.

At each wavelength reported here, photoelectron spectra of all energetically accessible valence states of BF_3 were recorded at $\theta=0^\circ$, 45° , and 90° . Figure 1 shows a typical set of data taken at a photon energy of $h\nu=23 \text{ eV}$. All three spectra are normalized so that the largest peak (third peak in the $\theta=0^\circ$ spectrum) has a value of 100. In the top frame, the six peaks are labeled by the symmetry of the orbital being ionized, based on the well-established valence configuration.²⁸⁻³² By careful inspection of Fig. 1, one can see that, at this wavelength, the β 's for peaks 1 and 5 are negative, the β for peak 2 is nearly isotropic, and the β 's for peaks 3 and 4 are positive.

At each angle of observation, the net counts in each photoelectron peak were summed, and the integrated counts were corrected for the transmission function of the electron spectrometer and a small $<4\%$ angular correction factor based on the aforementioned electron spectrometer angular calibration. The asymmetry parameter β was then determined for each peak by means of Eq. (1).

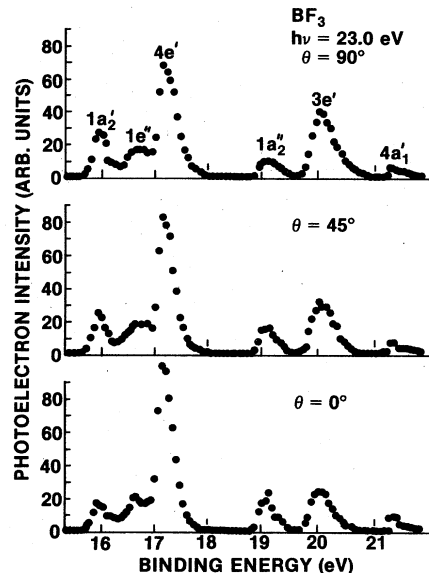


FIG. 1. Photoelectron spectra of BF_3 at $h\nu=23 \text{ eV}$ and $\theta=0^\circ$, 45° , and 90° . The normalization of the three spectra is internally consistent and set so that the maximum count rate (third peak of the $\theta=0^\circ$ spectrum) is equal to 100.

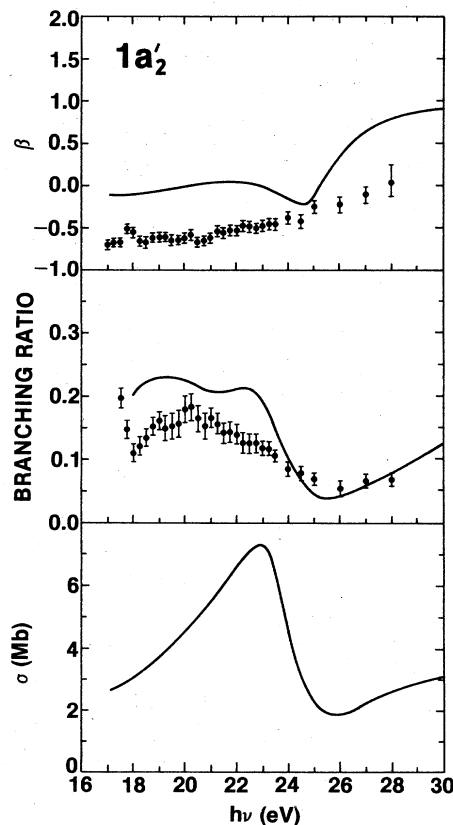


FIG. 2. Photoelectron asymmetry parameter, branching ratio, and partial cross section for photoionization of the $1a_2'$ orbital of BF_3 . Solid dots are the present data, and the solid curves are theoretical results from Ref. 20.

Photoionization branching ratios were then determined from the measured intensities and β values. Note that in Fig. 1, the $1e''$ and $4e'$ photoelectron bands (peaks 2 and 3) are not clearly resolved. In fact, recent theoretical work by Haller *et al.*³² indicate that a tail from the $1e''$ band runs under the $4e'$ band. As we do not know the actual shapes of the two bands, we have chosen to present the data in two ways. In one approach, the partially resolved band has been deconvoluted simply by separating the two peaks at the point of minimum intensity. In the second approach, we have reported the sum of the two peaks as a composite photoelectron band. This will be discussed further in Secs. III and IV. The errors quoted in the presentation of the results in Sec. III represent a combination of the statistical uncertainty of the integrated peak intensities, a propagation of errors from the calibration procedures, and the degree of agreement between the parameters deduced from the redundant set of measurements at three angles.

III. RESULTS

There are six occupied valence orbitals of BF_3 with ionization potentials in the energy range studied in this work. Starting with the outermost orbital, from the left in Fig. 1, the symmetries and vertical IP's are as follows:

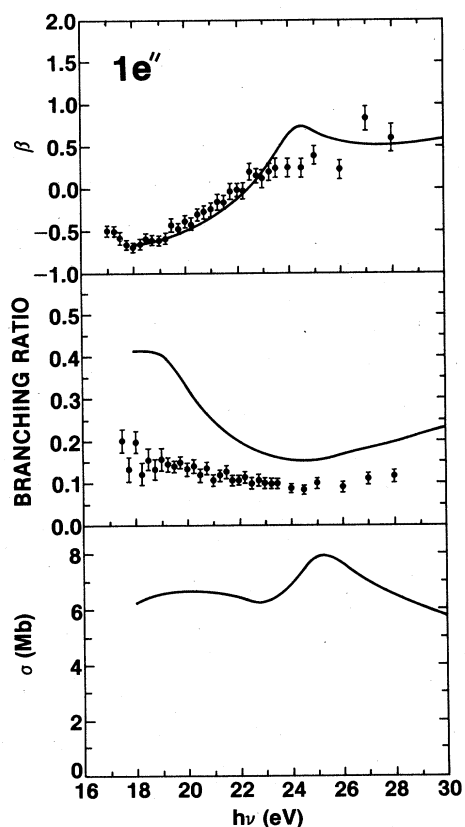


FIG. 3. Photoelectron asymmetry parameter, branching ratio, and partial cross section for photoionization of the $1e''$ orbital of BF_3 . Solid dots are the present data, and the solid curves are theoretical results from Ref. 20.

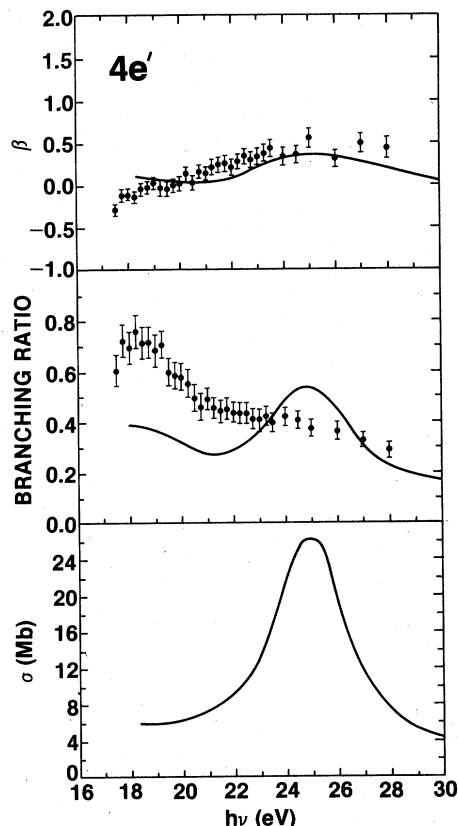


FIG. 4. Photoelectron asymmetry parameter, branching ratio, and partial cross section for photoionization of the $4e'$ orbital of BF_3 . Solid dots are the present data, and the solid curves are theoretical results from Ref. 20.

$1a'_2$ (15.96 eV), $1e''$ (16.70 eV), $4e'$ (17.12 eV), $1a''_2$ (19.14 eV), $3e'$ (20.12 eV), and $4a'_1$ (21.4 eV). Here the symmetry assignments are taken from Haller *et al.*³² and agree with most previous assignments.^{29–31} The vertical IP's are an average of several independent measurements,^{28–31} all of which are in close agreement.

The results are presented in Figs. 2–8 for each photoelectron peak and for a combination of the partially resolved $1e''$ and $4e'$ peaks (Fig. 5). Included with the experimental data are results of recent theoretical calculations²⁰ employing the multiple-scattering model.³³ The latter have not been folded with the finite instrumental resolution, but this does not affect the present comparison in any significant way. Each figure consists of three frames. The top frame presents the photoelectron asymmetry parameter, β , from the IP up to $h\nu=30$ eV. The middle frame shows the photoelectron branching ratio for each channel. In the lower frame, the calculated partial cross section is displayed. Unfortunately, the total absorption cross section of BF_3 is not known in this wavelength range, so we are unable to convert the measured branching ratios to partial cross sections. A photoionization mass spectrometry measurement³⁴ was made up to $h\nu\sim 20$ eV, but this wavelength range is too limited to be very helpful in the present discussion.

In the top frames of Figs. 2–8, we see the degree to

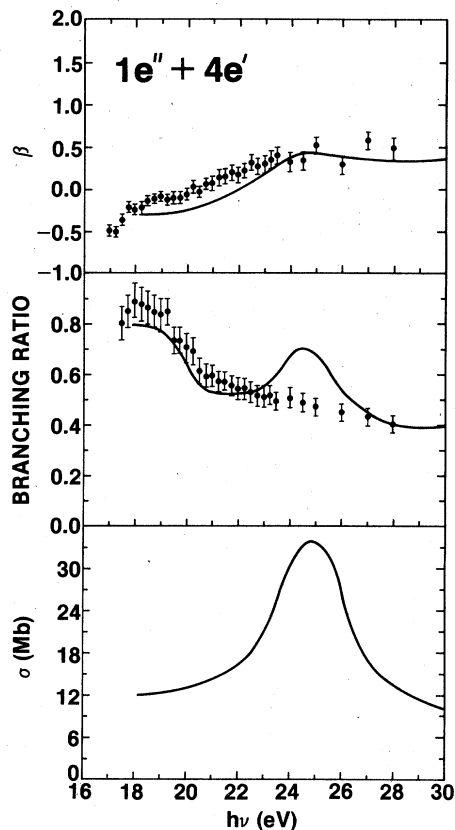


FIG. 5. Photoelectron asymmetry parameter, branching ratio, and partial cross section for photoionization of the $1e''$ and $4e'$ orbitals of BF_3 . Solid dots are the present data, and the solid curves are theoretical results from Ref. 20.

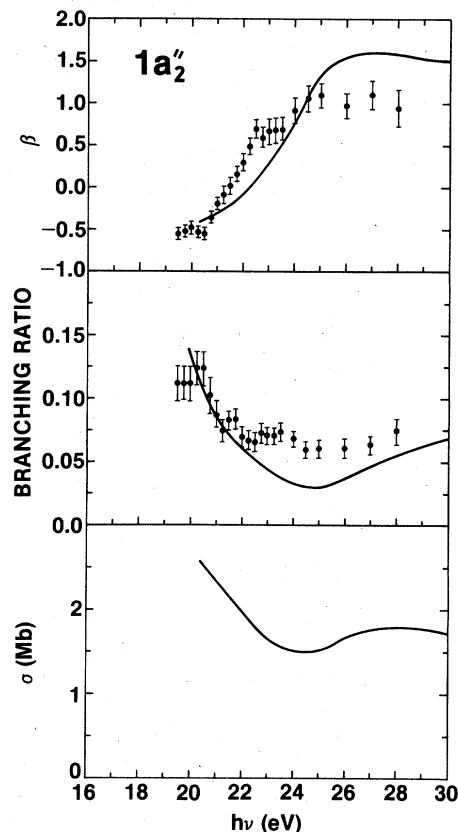


FIG. 6. Photoelectron asymmetry parameter, branching ratio, and partial cross section for photoionization of the $1a_2''$ orbital of BF_3 . Solid dots are the present data, and the solid curves are theoretical results from Ref. 20.

which the measured β 's agree with the predictions of the multiple scattering calculation. The results for the $1e''$, $4e'$, and $1a_2''$ orbitals (Figs. 3–6) show excellent agreement between experiment and theory. For the $1a_2'$ (Fig. 2) and $3e'$ (Fig. 7) orbitals, the experiment and theory agree fairly well in shape, but the magnitudes are different by $\sim 0.5 \beta$ units on the average, a difference not uncommon even in much simpler molecules. The poorest agreement is found for the $4a_1'$ orbital (Fig. 8), which is also by far the weakest channel. On the whole, the agreement is satisfactory, in view of the standards in the field, and it indicates that the theoretical results realistically reflect the gross photoionization dynamics of BF_3 . In comparing the present results with those¹⁰ for SF_6 , it is interesting to note that the present β 's tend to be rather anisotropic (ranging from $\beta < -0.5$ to $\beta \sim 1.5$), whereas those for the valence orbitals of SF_6 tended to gravitate strongly toward the isotropic value $\beta = 0$. This is not surprising, but it does show that the very simple isotropic pattern for $F2p$ -derived orbitals in SF_6 is not in any sense typical of highly coordinated fluorides.

The branching ratios are shown in the middle frames of Figs. 2–8. For the $1a_2'$ (Fig. 2) and $1a_2''$ (Fig. 6) cases, good agreement between theory and experiment is observed, both in shape and magnitude. For the overlapping

$1e''$ and $4e'$ orbitals, two discrepancies between theory and experiment emerge. Most obvious, the bump at $h\nu \sim 25$ eV in the calculated branching ratio for $4e'$ does not appear in the measured branching ratio. This will be discussed further in Sec. IV. The other discrepancy occurs on either side of this bump, where the measured branching ratios are lower than the theoretical curve for $1e''$ and higher than the theoretical curve for $4e'$. The reason this is noteworthy is that this is consistent with the results of Haller *et al.*³² who predict that the $1e''$ photoelectron band runs under the $4e'$ band and that a sizable fraction of its intensity is thereby covered up by the $4e'$ band. Our method of separating the intensity of the overlapping bands would have the effect of erroneously shifting intensity from the $1e''$ peak to the $4e'$ peak. In fact, when the two are summed in Fig. 5 the agreement away from the $h\nu \sim 25$ eV bump is remarkably good, adding some support to the prediction by Haller *et al.*³² Note that the separately determined β 's for these two channels should be much less sensitive to this issue. The remaining two channels reflect rather good agreement between theory and experiment. The $3e'$ branching ratio, in fact, reflects a maximum, similar in magnitude to, but slightly shifted from that in the theoretical curve. The $4a_1'$ branching ratio agrees well in shape with the theoretical

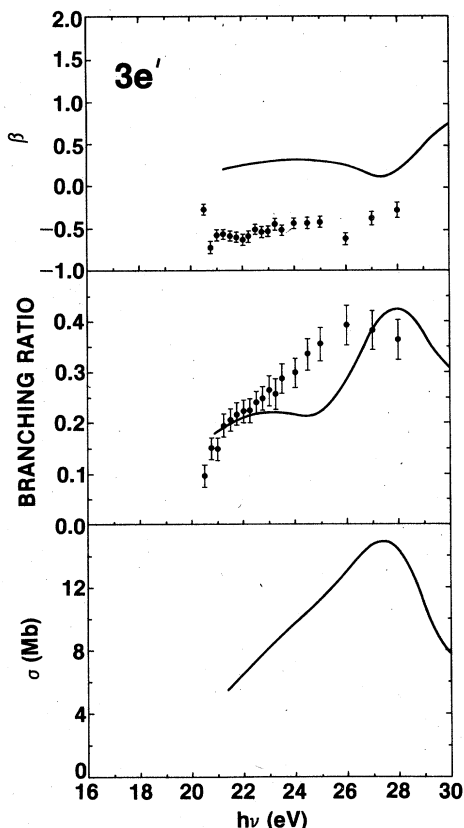


FIG. 7. Photoelectron asymmetry parameter, branching ratio, and partial cross section for photoionization of the $3e'$ orbital of BF_3 . Solid dots are the present data, and the solid curves are theoretical results from Ref. 20.

curve, both reflecting a sharp increase at high energy. The factor of 2 error in magnitude is not surprising in view of the very weak intensity in this channel just above its IP.

The bottom frames in Figs. 2–8 contain the partial cross sections produced by the theoretical calculation.²⁰ Comparison with experiment will require measurement of a total photoabsorption cross section, which, when multiplied by the present branching ratios, would yield experimental partial cross sections. Or, direct measurement by constant initial state photoelectron spectroscopy would produce the needed experimental data. As neither is presently available, the theoretical curves are included for discussion in Sec. IV, as partial cross sections and branching ratios present rather different views of the photoionization process. We anticipate ourselves by noting that the most definitive evidence for the e' shape resonance in valence-shell photoionization is likely to result from measurement of the $4e'$ partial cross section.

IV. DISCUSSION

The boron K -shell x-ray absorption spectrum^{4,15–21} displays two prominent features—an intense peak ~ 7 eV below the IP, and a broad (FWHM ~ 4 eV), intense peak centered at ~ 2.2 eV above the IP. Recent multiple-

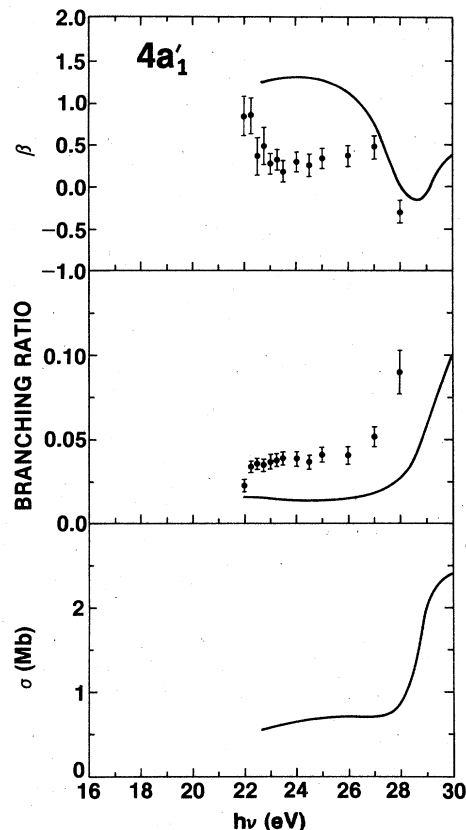


FIG. 8. Photoelectron asymmetry parameter, branching ratio, and partial cross section for photoionization of the $4a_1'$ orbital of BF_3 . Solid dots are the present data, and the solid curves are theoretical results from Ref. 20.

scattering calculations²⁰ show that these features can be understood at the independent electron level and that they correspond to transitions to a $2a_2''$ bound state and an e' shape resonance, respectively, in accordance with other interpretations.^{4,15–19,21} Since the e' shape resonance is a final-state feature, it should also be accessed in symmetry allowed transitions from the valence shells. One of the primary motivations of this work was to investigate the role of the e' resonance in valence-shell photoionization dynamics of BF_3 . Indeed, calculations²⁰ show that five of the six valence orbitals of BF_3 (all but the $1a_2''$) are connected to the e' continuum by dipole selection rules, and further, that the e' is predicted to have clearly visible effects. As so often happens, however, the valence-shell properties do not follow the independent-electron predictions as clearly as do the inner-shell properties. As we will show, rather good, but indirect, evidence for the e' shape resonance is given by the β 's, and the $3e'$ and $4a_1'$ branching ratios show direct evidence near the upper limit of our energy range. However, a predicted peak in the $4e'$ branching ratio is missing in the data, indicating the presence of interactions which are not adequately incorporated in the calculation.

Accordingly, it is important to have an independent way of estimating the location of the e' shape resonance in the valence-shell continua so as to establish the pres-

ence or absence of such effects. Fortunately, this can be fairly reliably done based on the position of the e' shape resonance in the inner-shell spectra, plus a kinetic-energy shift associated with differences in screening between a localized hole and a valence-shell hole. Examining well-characterized cases in N_2 , CO, and SF_6 , it is found that shape resonances experience a shift to higher kinetic energies when going from an inner-shell spectrum to a valence-shell spectrum. These shifts cluster around ~ 3 eV and always fall in the range 1–4 eV. Therefore, the e' shape resonance, which is centered at 2.2 eV kinetic energy in the boron K -shell spectrum, should fall in the 3–6 eV kinetic-energy range in the valence-shell spectra. As the calculation quoted here placed the resonance at ~ 8 -eV kinetic energy, the true resonance position should fall to the low-energy side of the predicted position. This means that the photon energy range studied in this work should suffice to investigate the role of the e' shape resonance in the six channels studied, though the resonance position in the $3e'$ and $4a'_1$ channels falls near the high-energy limit of the data reported here.

For completeness, we mention other states that will influence the valence-shell photoionization of BF_3 in this energy range. Multiple scattering model calculations²⁰ also predict a shape resonance in the a'_1 continuum, approximately 1–2 eV below the e' shape resonance. The a'_1 resonance derives from the trapping of p waves on the fluorine sites, as does the e' resonance, but it is not dipole allowed in boron K -shell photoexcitation and, hence, does not arise in earlier discussions involving inner-shell processes. Among the valence shells, the a'_1 continuum is dipole-allowed from the $4e'$, $1a''_2$, and $3e'$ initial states. According to the theoretical results,²⁰ the a'_1 resonance is masked by a much more intense e' resonance in the $4e'$ channel and is suppressed by a coincident zero in the dipole matrix element in the $1a''_2$ channel. However, in the $3e'$ channel, it is equal in strength and shifted slightly from the e' shape resonance. Therefore, the net resonant feature in the $3e'$ channel must be considered a composite resonance with significant contributions from shape resonances in both the e' and a'_1 continua. However, as the e' resonance is sharper, it still determines the peak position of the combined resonance feature in the $3e'$ partial cross section. For this reason, we will continue to refer to the e' resonance in what follows, although the likely contribution from the a'_1 resonance should be recognized.

Another possible class of states to consider is autoionizing states converging to all but the lowest IP. Although we do not detect any narrow structure in the data that would indicate autoionizing structure, channel interaction with the Rydberg states converging to the $1e''$ through $4a'_1$ thresholds may contribute to the failure to see features predicted from independent-electron calculations. Of particular interest is the possibility that transitions to the $2a''_2$ state (essentially a boron $2p_z$ orbital), so prominent in the boron K -shell spectra,^{15–21} might affect the present data. In the K -shell spectra, this peak is ~ 7 eV below the IP. If we assume a 2–3 eV shift for the valence-shell spectra, this state should not affect the present range, except possibly in the $4a'_1$ channel where it would fall at $h\nu \sim 17$ eV, to a first approximation. How-

ever, as known³⁵ from examples in both atoms and molecules, intrashell or intravalence transitions can undergo significant splitting and redistribution of oscillator strength to higher energies, relative to an independent electron picture. Although these possibilities must be recognized in considering the experimental results, we have no particular reason to believe that they play an important role in this case.

We now examine the data in Figs. 2–8 for the effects of the e' shape resonance. In doing so, we examine separately the β 's, branching ratios, and partial cross sections, as each reflects the photoionization dynamics in a different way. The β 's differ from the other two in that they contain information on the phases of the continuum wave functions. However, as seen in our earlier study¹⁰ of valence-shell photoionization of SF_6 , the branching ratios and partial cross sections also differ greatly in the way they display photoionization features. In the upper frames of Figs. 2–8, the gross shapes of the measured curves agree reasonably well with theory, and the agreement is excellent, in shape and magnitude, for the $1e''$, $4e'$, and $1a''_2$ channels. The e' shape resonance plays significant roles for all but the $1a''_2$ channel, so that one is tempted to consider this indirect evidence that the role of the e' shape resonance in this spectral range is observed and reasonably accounted for by the calculations. Turning to the branching ratios, we note fair to good agreement between experiment and theory for all except the $4e'$ channel. In particular, the broad maximum at $h\nu \sim 26$ eV in the $3e'$ branching ratio and the rising branching ratio at high photon energy for $4a'_1$ represent direct evidence for the e' shape resonance in those channels. Using the $3e'$ branching ratio data, one can place the resonance position at $h\nu \sim 26$ eV, corresponding to a kinetic energy of ~ 6 eV, in accord with expectations. The surprising aspect of these results is the absence of an e' -induced peak at $h\nu \sim 25$ eV in the $4e'$ branching ratio. This will be discussed further below. The partial cross sections in the bottom frames are presently available from theory only. They show that the e' shape resonance will emerge much more clearly when presented in this form. In particular, the peak at $h\nu \sim 25$ eV in the $4e'$ partial cross section is predicted to have a much greater contrast ratio than the same feature in the branching ratio. Similarly, the e' resonance will be displayed more clearly in the partial cross section than in the branching ratio for the $1e''$ and the $1a''_2$ channels as well. For the $3e'$ and $4a'_1$ channels, both parameters display the resonance equally clearly, and, in fact, these are the two cases in which the e' shape resonance can be observed in the present branching ratio data. Recall that in the $3e'$ channel, the a'_1 shape resonance also contributes to the resonant feature at $h\nu \sim 26$ eV, as discussed earlier.

The failure to observe in valence-shell properties a final-state resonance well established in inner-shell spectra is not at all unprecedented. In SF_6 , an e_g shape resonance causes an intense peak ~ 15 eV above the sulfur $L_{2,3}$ IP, (see Refs. 2–7) but is absent from valence-shell partial cross sections^{8,9} where its presence is predicted by theory. An even more subtle example is the $4\sigma_g$ ionization channel of CO_2 which was predicted^{36–41} to access a strong σ_u

shape resonance at ~ 20 eV kinetic energy. Nothing resembling the predicted resonance feature was observed in partial cross section measurements;^{42,43} however, a predicted dip in the β curve^{37,38,40,41} at the resonance energy was subsequently observed experimentally,⁴⁴ giving evidence that the "missing" resonance existed, even though its manifestation in the partial cross section was drastically reduced by some as yet unknown interaction. So we add to this list the $4e'$ channel in BF_3 which has a β curve consistent with theory but fails to show the branching ratio feature resulting from the presence of the e' shape resonance.

Without further evidence, we can only speculate as to possible causes for the missing e' feature: First, it is well known that multiple-scattering model calculations produce shape resonance profiles that are too narrow and too intense. Hence, effects such as intrachannel coupling³⁵ and/or averaging over vibrational motion³⁸ will tend to smear out and diminish a shape resonant feature. Nevertheless, the feature should still be observable in the partial cross section, even if it is absent from the branching ratio. This is certainly possible in the present case since, if the total photoabsorption cross section peaks near $h\nu \sim 25$ eV, a flat branching ratio will produce a peak in the partial cross section. Second, interchannel coupling (either discrete-continuum or continuum-continuum) with other underlying valence channels can significantly alter the predictions based on an independent-electron theory. For instance, continuum-continuum coupling is believed to strongly influence valence-shell photoionization in SF_6 .¹⁰ Such channel interaction can be expected to be stronger among valence channels with their closely spaced IP's. The good agreement found for the β results tend to argue against this possibility. Note that in SF_6 the β results¹⁰ showed very poor agreement between experiment and theory for the affected channels. Third, vibronic coupling has been shown³² to play a very important role in photoelectron spectra of BF_3 . This and other vibrational effects are excluded from the calculations²⁰ quoted here. We do not know how to assess the importance of such ef-

fects at this time. Other possibilities clearly exist, but these examples serve to indicate the types of mechanisms which may be causing the reduction of certain shape resonance effects in valence-shell spectra. Taken together, the examples quoted in CO_2 , BF_3 , and SF_6 pose a major challenge to our understanding of shape resonance phenomena.

We conclude by suggesting future work to help clarify the role of the e' shape resonance in BF_3 photoionization processes. Clearly it is very important to measure the partial photoionization cross sections for the valence shells to complete the comparisons begun in Figs. 2–8. This would require the total photoabsorption cross section in order to convert the present branching ratios to partial cross sections, or that a constant-initial-state photoelectron measurement be made on the valence shells of BF_3 . New measurements at higher energy would also be very valuable, both to complete the study of the e' features at the high-energy limit of the present data, and to investigate the role of the e' resonance in the inner-valence $3a'_1$ and $2e'$ orbital whose energies are predicted to fall near $h\nu \sim 40$ – 43 eV.

Note added in proof. A recent experimental study by Roy *et al.*⁴⁵ has provided clear evidence for the "missing" σ_u shape resonance in the $4\sigma_g$ channel of CO_2 , discussed in the last section. It had been overlooked mainly because it was smaller in amplitude and occurred at nearly 10 eV lower energy than predicted by the most accurate calculations.

ACKNOWLEDGMENTS

We wish to thank R. P. Madden and the staff of the National Bureau of Standards SURF-II facility for their support and assistance during the course of this work. We are also grateful to Dan Dill and Jeff Stephens for making the results of Ref. 20 available in digital form. This work was supported by the Office of Naval Research, by the U.S. Department of Energy, and by the North Atlantic Treaty Organization (Grant No. 1939).

*Present address: Daresbury Laboratory, Science Research Council, Daresbury, Warrington WA44AD, England.

¹J. L. Dehmer, D. Dill, and A. C. Parr, in *Photophysics and Photochemistry in the Vacuum Ultraviolet*, edited by S. McGlynn, G. Findley, and R. Huebner (Reidel, Dordrecht, 1984).

²T. M. Zimkina and V. A. Fomichev, Dokl. Akad. Nauk SSSR **169**, 1304 (1966) [Sov. Phys.—Dokl. **11**, 726 (1966)].

³T. M. Zimkina and A. C. Vinogradov, J. Phys. (Paris) Colloq. **32**, 3 (1971).

⁴J. L. Dehmer, J. Chem. Phys. **56**, 4496 (1972).

⁵F. A. Gianturco, C. Guidotti, and U. Lamanna, J. Chem. Phys. **57**, 840 (1972).

⁶R. E. LaVilla, J. Chem. Phys. **57**, 899 (1972).

⁷D. Blechschmidt, R. Haensel, E. E. Koch, U. Nielsen, and T. Sagawa, Chem. Phys. Lett. **14**, 33 (1972).

⁸T. Gustafsson, Phys. Rev. A **18**, 1481 (1978).

⁹H. J. Levinson, T. Gustafsson, and P. Soven, Phys. Rev. A **19**, 1089 (1979).

¹⁰J. L. Dehmer, A. C. Parr, S. Wallace, and D. Dill, Phys. Rev. A **26**, 3283 (1982).

¹¹P. Morin, I. Nenner, M. Y. Adam, M. J. Hubin-Franskin, J. Delwiche, H. Lefebvre-Brion, and A. Giusti-Suzor, Chem. Phys. Lett. **92**, 609 (1982).

¹²Z. H. Levine and P. Soven, Phys. Rev. Lett. **50**, 2074 (1983).

¹³L. S. Cederbaum, W. Domcke, J. Schirmer, and W. von Niessen, Phys. Scr. **21**, 481 (1980).

¹⁴S. Krummacher, V. Schmidt, and F. Wuilleumier, J. Phys. B **13**, 3993 (1980).

¹⁵V. A. Fomichev, Fiz. Tverd. Tela (Leningrad) **9**, 3167 (1967) [Sov. Phys.—Solid State **9**, 2496 (1968)].

¹⁶V. A. Fomichev and R. L. Barinskii, J. Struct. Chem. **11**, 810 (1970).

¹⁷W. Hayes and F. C. Brown, J. Phys. B **4**, L85 (1971).

- ¹⁸L. N. Mazalov, F. Kh. Gel'mukhanov, and V. M. Chermoshentsev, *J. Struct. Chem.* **15** 1099 (1974).
- ¹⁹M. B. Robin, *Chem. Phys. Lett.* **31**, 140 (1975).
- ²⁰J. R. Swanson, D. Dill, and J. L. Dehmer, *J. Chem. Phys.* **75**, 619 (1981).
- ²¹E. Ishiguro, S. Iwata, Y. Suzuki, A. Mikuni, and T. Sasaki, *J. Phys. B* **15**, 1841 (1982).
- ²²A. C. Parr, R. L. Stockbauer, B. E. Cole, D. L. Ederer, J. L. Dehmer, and J. B. West, *Nucl. Instrum. Methods* **172**, 357 (1980).
- ²³D. L. Ederer, B. E. Cole, and J. B. West, *Nucl. Instrum. Methods* **172**, 185 (1980).
- ²⁴G. V. Marr and J. B. West, *At. Data Nucl. Data Tables* **18**, 497 (1976).
- ²⁵J. L. Dehmer, W. A. Chupka, J. Berkowitz, and W. T. Jivery, *Phys. Rev. A* **12**, 1966 (1975).
- ²⁶J. Kreile and A. Schweig, *J. Electron Spectrosc.* **20**, 191 (1980).
- ²⁷D. M. P. Holland, A. C. Parr, D. L. Ederer, J. L. Dehmer, and J. B. West, *Nucl. Instrum. Methods* **195**, 331 (1982).
- ²⁸A. W. Potts, H. J. Lempka, D. G. Streets, and W. C. Price, *Philos. Trans. R. Soc. London Ser. A* **268**, 59 (1970).
- ²⁹C. F. Batten, J. A. Taylor, B. P. Tsai, and G. G. Meisels, *J. Chem. Phys.* **69**, 2547 (1978).
- ³⁰K. Kimura, S. Katsumata, Y. Achiba, T. Yamazaki, and S. Iwata, *Handbook of HeI Photoelectron Spectra of Fundamental Organic Molecules*, (Japan Scientific Societies Press, Tokyo and Halsted Press, New York, 1981).
- ³¹L. Åsbrink, A. Svenson, W. von Niessen, and G. Bieri, *J. Electron Spectrosc.* **24**, 293 (1981).
- ³²E. Haller, H. Köppel, L. S. Cederbaum, W. von Niessen, and G. Bieri, *J. Chem. Phys.* **78**, 1359 (1983).
- ³³The theoretical curves have been adjusted to correspond to the level ordering and the IPs listed in the last paragraph. Note that Ref. 20 adopted the incorrect experimental ordering for the closely spaced $4e'$ and $1e''$ levels.
- ³⁴V. H. Dibeler and S. K. Liston, *Inorg. Chem.* **7**, 1742 (1968).
- ³⁵See, e.g., Z. H. Levine and P. Soven, *Phys. Rev. A* **29**, 625 (1984).
- ³⁶J. R. Swanson, D. Dill, and J. L. Dehmer, *J. Phys. B* **13**, L231 (1980).
- ³⁷F. Grimm, T. A. Carlson, W. B. Dress, P. Argon, J. O. Thomson, and J. W. Davenport, *J. Chem. Phys.* **72**, 3041 (1980).
- ³⁸J. R. Swanson, D. Dill, and J. L. Dehmer, *J. Phys. B* **14**, L207 (1981).
- ³⁹N. Padiyal, G. Csanak, B. V. McKoy, and P. W. Langhoff, *Phys. Rev. A* **23**, 218 (1981).
- ⁴⁰R. R. Lucchese and B. V. McKoy, *Phys. Rev. A* **26**, 1406 (1982).
- ⁴¹R. R. Lucchese and B. V. McKoy, *Phys. Rev. A* **26**, 1992 (1982).
- ⁴²C. E. Brion and K. H. Tan, *Chem. Phys.* **34**, 141 (1978).
- ⁴³T. Gustafsson, E. W. Plummer, D. E. Eastman, and W. Gudat, *Phys. Rev. A* **17**, 175 (1978).
- ⁴⁴T. A. Carlson, M. O. Krause, F. A. Grimm, J. D. Allen, D. Mehaffy, P. R. Keller, and J. W. Taylor, *Phys. Rev. A* **23**, 3316 (1981).
- ⁴⁵P. Roy, I. Nenner, M. Y. Adam, J. Delwiche, M. J. Hubin Franskin, P. Lablanquie, and D. Roy, *Chem. Phys. Lett.* (to be published).